JACS
JOURNAL OF THE AMERICAN CHEMICAL SOCIETY
Article
pubs.acs.org/JACS

Two Types of Water at the Water–Surfactant Interface Revealed by Time-Resolved Vibrational Spectroscopy

Ruth A. Livingstone,* Yuki Nagata, Mischa Bonn, and Ellen H. G. Backus

Max Planck Institute for Polymer Research, Ackermannweg 10, 55128 Mainz, Germany

Supporting Information

ABSTRACT: The surfactant sodium dodecyl sulfate (SDS) is widely used as a detergent for both domestic and industrial applications. It forms a self-assembled monolayer on the surface of water. We report a microscopic model for the interaction between the surfactant and water and between water molecules at the interface, revealed using static and time-resolved two-dimensional sum frequency generation spectroscopy. Two distinct subensembles of water in the presence of this negatively charged SDS surfactant have been identified: those close to the SDS headgroup having fairly isolated O–H groups, i.e., localized O–H stretch vibrations, and those whose O–H stretch vibrations are delocalized, i.e., shared between multiple O–H bonds. The two subensembles are coupled, with subpicosecond energy transfer occurring between them. This is markedly different from O–H bonds at the air–water interface, which are less heterogeneous, and indicates that the water molecules that interact with the surfactant headgroups have hydrogen-bonding properties different from those of water molecules interacting with the other water molecules.

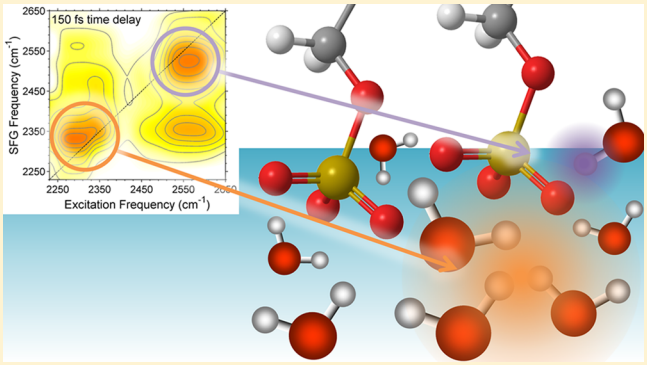

INTRODUCTION

Surfactants play an important role in many industrial and biological applications.[1] They form a monolayer on the surface of water, reducing the surface tension of water. In the lungs this allows the alveoli to maximize their surface area and function without collapsing.[2] In industry this helps the water to more effectively wet a surface—which is useful for, among other things, lubrication and cleaning applications. The surfactant sodium dodecyl sulfate (SDS), shown in Figure 1, is widely used as a detergent.[1] In products such as shampoo, toothpaste, and industrial cleaners, it is released in large quantities into the environment. This anionic surfactant is also used by biologists, for example, for unfolding proteins to prepare them for electrophoresis in the popular SDS–PAGE (polyacrylamide gel electrophoresis) method,[3] and for extracting DNA fragments.[4] Despite its relevance, it has been challenging to characterize the molecular-level interactions of the water–SDS–air mixture, to determine to what extent the electrostatic charge and the molecular interactions affect the microscopic structure of the interfacial water molecules.

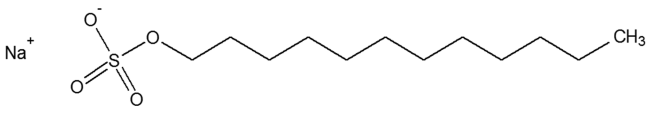

Figure 1. Chemical structure of the sodium dodecyl sulfate (SDS) molecule.

In bulk water the water molecules are hydrogen bonded to one another; at the water–air interface this hydrogen-bonding network is disrupted due to the absence of water molecules above the interface. When SDS is added to water, the interfacial water molecules can form hydrogen bonds with the headgroups of the surfactant SDS molecules. This reduces the surface tension of the water solution from 72 to 39 mN/m for sufficiently high concentrations at room temperature and pressure.[5] Sum frequency generation (SFG) spectroscopy techniques can selectively probe vibrational responses from both water and surfactant molecules specifically at the interface, which have a net nonzero orientation along the surface normal. It is therefore uniquely suited to studying the surface properties of solids and liquids.[6−8] Several SFG studies on both positively and negatively charged surfactant–water interfaces have been reported, some focusing on the surfactant molecules,[9−11] others looking at the water molecules at the interface with surfactants[3] or lipids—a class of biological surfactants.[4,12,13] It has been found that charged surfactants induce an alignment of the water molecules below them, while uncharged surfactants do not have a strong effect on the interfacial ordering of the water.[14,15] The negative charge on the SDS headgroup aligns the water molecules to have their oxygen molecules facing toward the bulk.[14] This alignment is thought to arise either from the large electrostatic fields present at the interface[4,14−16] or from influencing the hydrogen-bonding network of the water

Received: August 4, 2015
Published: November 6, 2015

DOI: 10.1021/jacs.5b07845
J. Am. Chem. Soc. 2015, 137, 14912−14919

molecules.[17] It has been reported that an increase of the SDS concentration at the interface does not affect the orientation of the headgroup,[11] while the hydrocarbon tail rearranges from a disordered, largely in-plane conformation at low concentrations to standing vertically at high concentrations.[18,19] Above the critical micelle concentration (cmc), SDS additionally forms micelles in solution,[20] the surface monolayer contains much less impurities,[21,22] and it is less affected by temperature fluctuations.[20] The cmc is affected by temperature[20,23] and the presence of salts[20,24] and surface-active impurities.[5,25] While these macroscopic studies have provided many insights into the thermodynamics of the SDS–water interface, the challenge is to characterize the newly formed water–SDS hydrogen bond at the water surface, and understand how this affects the interfacial water region at a molecular level.

To elucidate the structure of water molecules at specifically the interface, we use a combination of SFG and two-dimensional SFG (2D-SFG).[26] 2D-SFG is the surface analogue of 2D-IR (IR = infrared),[27] which has been successfully used to study water within surfactant micelles of various dimensions.[28−32] 2D-SFG is an extension of the SFG technique by adding a pump pulse and allows study of how different vibrational modes are coupled, how vibrational energy is exchanged between molecules, as well as how fast molecules lose memory of orientation and exchange their hydrogen bond partners. The subpicosecond resolution of this technique allows one to watch the dynamics of the molecules close to the time scale of the molecular motion itself. Time-resolved pump–probe studies on a range of lipids have found that water molecules with different hydrogen bond strengths relax differently after excitation—more weakly hydrogen bonded water molecules decaying to the ground state on an approximately 3 times longer time scale.[33,34]

Nevertheless, the structure of the interfacial water near the SDS monolayer has not been successfully related to the SFG signatures until now. There has been some discussion on the assignment of the two peaks in the O–H stretch region seen in almost all interfacial aqueous systems,[12,35−37] variously assuming two types of water, “icelike” and “liquidlike” water;[35] assuming one type of water, with splitting due to Fermi resonance;[12,26] or assigning the two peaks to those water molecules adjacent to and below the surfactant, respectively.[38] 2D-SFG on water at the positively charged surfactant interface shows cross-peaks due to the Fermi resonance that disappear upon isotopic dilution.[39] In this paper, we report static SFG and time-resolved 2D-SFG measurements at the water–SDS–air interface for various concentrations of H_2O–D_2O mixtures. We took great care to ensure that the monolayer consisted solely of SDS, and not one of its degradation products (see the Experimental Methods and Supporting Information). Our results allow us to establish a solid model for the structure and dynamics of interfacial water at the water–SDS interface, which may be generally extended to other negatively charged water–hydrophilic interfaces. Specifically, we identify the vibrational signatures of interfacial water and show that the SDS monolayer gives rise to two distinct water environments at the interface.

RESULTS AND DISCUSSION

The O–H stretch vibrational frequency of H_2O (or O–D stretch in the case of D_2O) is affected by the hydrogen bond strength between the water molecule and its surrounding environment. Strong hydrogen bonds result in lower O–H stretch frequencies,[40] so that the vibrational SFG spectra in this region give insight into the hydrogen bond network and the local environment of the water molecules at aqueous interfaces. Static SFG spectra in the O–D stretching region for the water–air interface are shown in Figure 2a. The SFG features at this

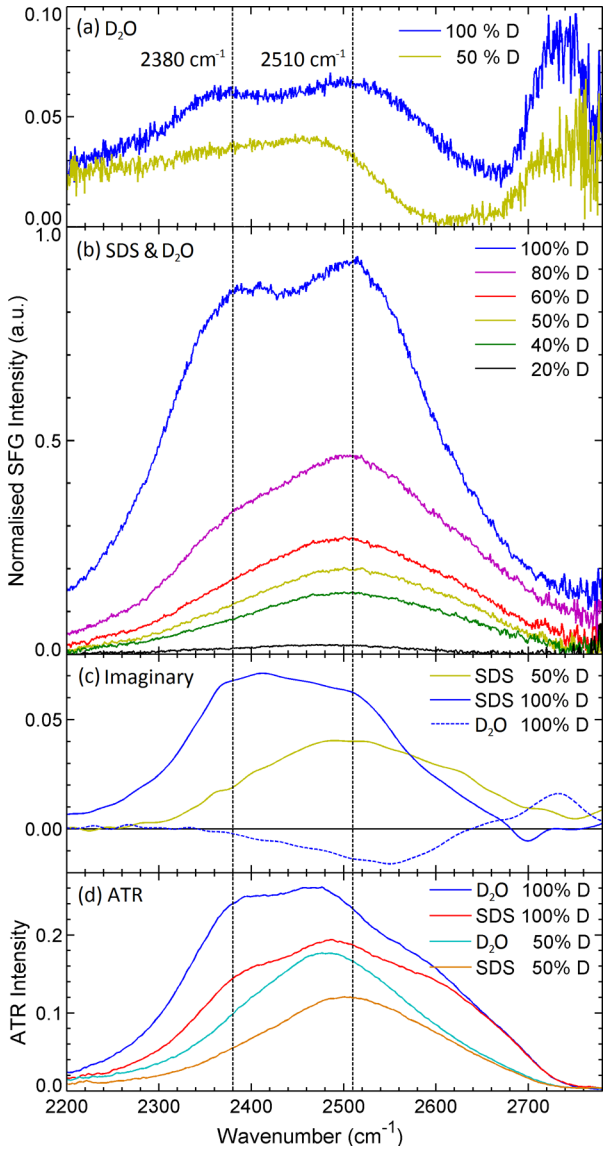

Figure 2. Static spectra of the O–D stretch region of water with and without surfactant, and at different isotopic dilutions. The legends show the percentage of D/(D + H) atoms in the solution. (b) and (c) Static SFG spectra of the water–surfactant–air interface at various isotopic dilutions. (a) and (c) SFG spectra for the bare water–air interface for comparison. (a) and (b) show the $|\chi^{(2)}|^2$ SFG signal, while (c) shows the imaginary part of the $\chi^{(2)}$ signal. (d) ATR spectra of both pure water (blue/cyan) and the water/SDS slurry (red/orange).

interface are well characterized.[35,41] The relatively sharp “free O–D” feature, seen in D_2O at 2750 cm^{-1}, corresponds to those O–D bonds that are pointing out of the surface.[35] These bonds vibrate at a high frequency due to the absence of hydrogen bond acceptors. In contrast, the hydrogen-bonded O–D groups have much broader features at the lower frequencies: two broad peaks centered around 2380 and 2510 cm^{-1}. These peaks come from the vibrational energy level splitting for the O–D stretch mode due to its intramolecular coupling to an overtone of the

DOI: 10.1021/jacs.5b07845
J. Am. Chem. Soc. 2015, 137, 14912−14919

bending mode (Fermi resonance)[36] and/or due to intermolecular coupling.[38] Such coupling is evident from the SFG spectrum for the isotopically diluted water: upon isotopic dilution the coupling is much reduced, resulting in the two peaks changing to one broad peak centered at 2480 cm^{-1}. This can be seen in the SFG spectrum for the 50% concentration of H_2O in D_2O (yellow line in Figure 2a).

When we turn to the water−surfactant SFG spectra, Figure 2b, initially the hydrogen-bonded O−D stretch region (2200−2600 cm^{-1}) looks very similar to that of the bare water−air interface for the neat D_2O case. A broad peak with a dip in the middle is seen for the hydrogen-bonded water, comparable to the broad peak seen for the bare interface. In contrast to the water−air interface, the free O−D peak is not present at the water−SDS interface, because the SDS molecules forming a monolayer over the surface provide adequate hydrogen bond acceptors for the interfacial water molecules. Moreover, the SFG signal intensity is more than 10 times stronger compared to that of the water−air interface, because the water molecules are aligned by the negative charge on the SDS headgroup, which enhances the signal. When we compare the spectra of the isotopically diluted water, however, we see that the response of bonded O−D groups beneath SDS is different from that of bare water. The peak at 2380 cm^{-1} is reduced in intensity, but the remaining peak does not shift to 2480 cm^{-1} as seen for bare water but remains centered at 2510 cm^{-1}. When we look at the imaginary part of the $\chi^{(2)}$ signal (Figure 2c obtained by phase-sensitive (heterodyne) SFG spectroscopy), we see essentially the same spectra at the water−SDS interface as those obtained with conventional (homodyne) spectroscopy in Figure 2b. This confirms that the SFG spectra at this water−surfactant interface are not affected by the complex interference of the positive and negative bands such as those at the water−air interface, and thus, we can conclude that the conventional SFG spectra are adequate to monitor the vibrational dynamics. As will be shown below, the intensity of the two O−D peaks as a function of isotopic dilution can provide useful information about the nature of the interfacial vibrations. H_2O, HDO, and D_2O have slightly different frequency-dependent refractive indices, resulting in variations in the local field at the interface as described by the Fresnel factors. To ensure that the changes in the spectra are only due to the changes in the water vibrations, not changes in the local field, we corrected our spectra for the Fresnel factors before fitting (see the Supporting Information for more details). The two peaks were fit using the following equation, which accounts for both the resonant ($\chi^{(2)}_{RES}$) and the nonresonant ($\chi^{(2)}_{NR}$) SFG components:

$$|\chi^{(2)}|^2 = |\chi^{(2)}_{NR} + \chi^{(2)}_{RES}|^2 = \left| A_{NR} e^{i\varphi_{NR}} + \sum_n \frac{A_n}{\omega_n - \omega_{IR} - i/2\Gamma_n} \right|^2 \quad (1)$$

The nonresonant component was fitted with amplitude A_{NR} and phase φ_{NR}. It was found that, for this water−surfactant interface, the nonresonant amplitude required to fit the spectra was negligible at all isotopic dilutions, which is another reason why conventional instead of phase-sensitive SFG can be used. We used two Lorentzian peaks ($n = 2$) centered at ω_1 = 2510 cm^{-1} and ω_2 = 2380 cm^{-1}, with widths of $\Gamma_1 = \Gamma_2$ = 170 cm^{-1}. The amplitude (A_n) of the two Lorentzian curves required to fit the two peaks as a function of isotopic dilution are plotted in Figure 3. These amplitudes were then fitted with the equation

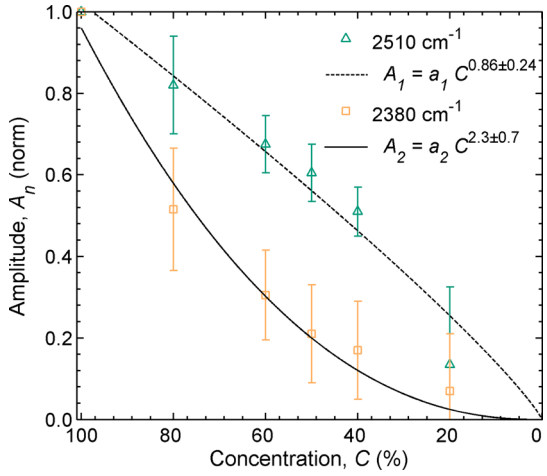

Figure 3. Amplitudes of the two peaks in the static SFG spectra as a function of isotopic dilution (% D/(D + H), with associated fits. The error bars depict the variance in the fit by using different fit parameters.

$A_n = aC^p$, where C is the relative concentration of deuterium atoms (D/(D + H)), a is a scaling factor, and p is the exponent. While the amplitude of the 2510 cm^{-1} peak, A_1, decreases in a (more or less) linear manner expected for vibrations localized on one bond ($p = 1$ within experimental error), the amplitude at 2380 cm^{-1}, A_2, is clearly nonlinear ($p = 2.3$). This nonlinear behavior can be accounted for by considering the intra/intermolecular couplings. It is known that these couplings can delocalize the vibrational quanta within the first hydration shell of water molecules[41−43] and shift the O−D stretching mode peak to lower frequencies.[44] Thus, the frequency of 2380 cm^{-1} observed here is consistent with the frequency variation observed in bulk IR spectra. This delocalization can occur, for example, over the two bonds in the same molecule, or over several adjacent molecules.[44]

To assign the two SFG peaks, we look at the possible physical causes for two different water environments at the interface. It has been reported that water O−H bonds in the presence of an anion vibrate at higher frequencies due to the electric fields involved.[45] The high-frequency peak could then originate from those interfacial water molecules close to the negatively charged surfactant headgroup. Simulations[38,46,47] have further shown that water might be present close to the hydrophobic tails. These molecules will be more weakly hydrogen bonded compared to bulk water and thus exhibit relatively high O−D stretch frequencies. In any case, water in contact with SDS is expected to be blue-shifted and so more isolated from the surrounding water molecules.[38] To help back up this assignment, we have measured the attenuated total internal reflection (ATR) spectra of a water/SDS slurry. In this slurry the SDS concentration was extremely high (27 water molecules for every SDS molecule), so many water molecules were in contact with an SDS molecule, in this way the water−SDS interactions could be examined with this technique, which is not surface sensitive. The ATR spectra (Figure 2d) show that the water O−D stretch frequency in the presence of SDS is blue-shifted, with relatively high spectral intensity around 2510 cm^{-1}, and lower intensity around the 2380 cm^{-1} peak. This is additional evidence that the localized vibration around 2510 cm^{-1} originates from O−D groups in direct contact with the SDS monolayer. Now we look at the lower frequency peak: it is

DOI: 10.1021/jacs.5b07845
J. Am. Chem. Soc. 2015, 137, 14912−14919

known that water molecules underneath a charged monolayer become aligned.[14] This alignment increases the hydrogen bond strengths, shifting the O−H vibration to lower frequencies.[36,38] This alignment may also increase the probability of delocalized vibrations involving more than one molecule.[41,48] We therefore suggest the 2380 cm^{-1} peak is a delocalized O−D stretch vibration of the aligned water molecules below the surfactant monolayer. While intermolecular coupling provides a sufficient explanation of the observed spectroscopy, we cannot exclude that part of the double peak behavior originates from intramolecular (i.e., Fermi resonance) coupling. These static spectra have given us useful new information about the two peaks in this interfacial water. However, these measurements have not told anything about how these two species interact at the interface. Are they isolated from each other, or is there energy transfer or structural diffusion between them? To answer these questions, we turn to time-resolved 2D techniques.

Time-resolved 2D-SFG spectroscopy is a powerful technique that can give us insight into the water molecules' vibrational dynamics, energy transfer, species transfer, and coupling. In such an experiment pump-induced changes in the SFG signal are plotted as a function of the pump and probe frequencies. This results in a 2D plot for each pump−probe time delay. A signal appearing on the diagonal of the 2D spectrum indicates molecules that have become excited to a specific vibrational state, and are still vibrating in that same state. The 2D spectrum will show off-diagonal "cross-peaks" if there are two coupled types of vibrations, where the population can easily move from one state to another, or anharmonic coupling between the two states shifts the frequency of the one state upon excitation of the other. In contrast to 2D techniques such as 2D-IR,[49] or phase-resolved, heterodyne-detected 2D-SFG,[39] the 1−2 vibrational transition does in general not contribute to the 2D spectrum; only the 0−1 transition is observed in the conventionally detected 2D-SFG technique used here. This is because the conventionally detected SFG intensity is proportional to $|\chi^{(2)}|^2$. Because of the squared nature of the process, SFG signals from excited states are so small as to be negligible.[50] If the 1−2 signal interferes with either the 0−1 or nonresonant signal, self-heterodyning effects could allow it to be observed. In the experiments performed here the nonresonant signal is negligible (as discussed above). Moreover, the anharmonicity of water is large (270 cm^{-1})[51] so that self-heterodyning of the 1−2 transition by the 0−1 transition will not take place. The disadvantage of the conventional SFG technique is that the spectra contain contributions from both the real and the imaginary parts of the signal, but this effect can be readily modeled using eq 1, especially given that the nonresonant signal is negligibly small, so that the conventional SFG spectra closely resemble the imaginary spectra (Figure 2b,c). As such, any distortions in the 2D spectra will be minor and should not affect our conclusions. This technique has previously been used to help understand the water−air interface.[7,52,53] The pure water interface shows no distinct cross-peaks within the hydrogen-bonded O−D region discussed here. The lack of clear cross-peaks for the water−air interface vibrational spectrum indicates that either the two modes are fully decoupled or the two peaks originate from only one type of vibration. The latter explanation is consistent with the conclusions drawn from the static SFG spectra (Figure 2a), showing that at the water−air interface the two peaks originate from the Fermi resonance.[36] In this picture, the two-peak response appears because one continuum of stretch states is split by the overtone of the band mode into two seemingly different bands that, however, originate from the same vibrational state.

The 2D-SFG spectra (pumped−unpumped) for the O−D stretch mode of the water molecules under SDS at selected pump−probe time delays are shown in Figure 4. In panels a−c

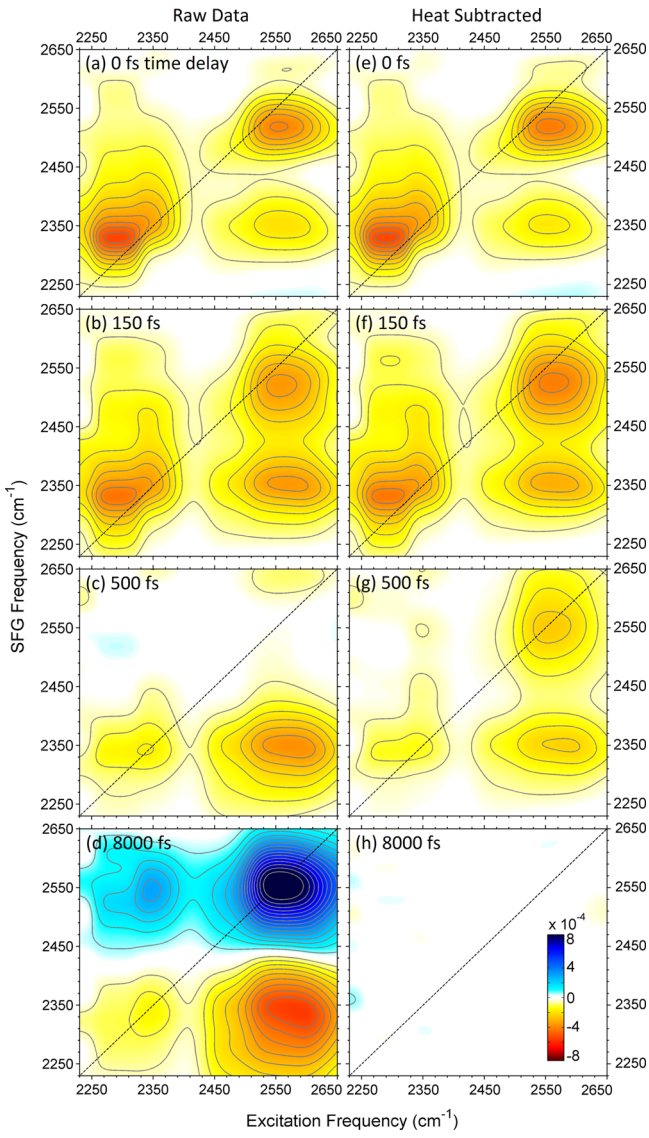

Figure 4. 2D-SFG spectra (pumped−unpumped) at selected pump−probe time delays. The first column (a−d) shows the as-collected data. In the second column (e−h) we have subtracted an approximation of the signal due to pump heating to more clearly observe the underlying dynamics. The dotted line shows where the detection frequency equals the excitation frequency. (Note that a -5×10^{-4} intensity corresponds to approximately 15% bleach.)

we can see two well-separated peaks along the diagonal and two cross-peaks lying off the diagonal. Figure 4d shows the signal at long delay times, which reflects the surface at elevated temperature, after the vibrational excitation has been fully thermalized. As a result of the pump-induced temperature increase, the O−H stretch vibrational response is blue-shifted for the interfacial water as well as the bulk water, due to a weakening of the hydrogen bonds.[54] The difference spectrum

DOI: 10.1021/jacs.5b07845
J. Am. Chem. Soc. 2015, 137, 14912−14919

(before and after excitation) reflects this blue shift, showing a characteristic positive response and negative response in the spectrum. This heat signal increases as a function of the pump–probe delay time, and the dynamics of the vibrational relaxation to the hot ground state can be modeled by coupled differential equations, as explained below. This model can be used, in combination with the thermalized spectrum collected at long pump–probe time delays, to correct the signal for the heating contribution at each different time delay. This approximation allows us to extract reconstituted 2D spectra without the strong heat signature distorting the features (Figure 4e–h). Subtracting the intensity signals, which are given by the squares of the susceptibilities, could introduce artifacts due to cross-terms between the susceptibilities of the vibrationally excited states and the hot ground state. For this reason the heat-subtracted 2D spectra are not used for any quantitative analysis. The two diagonal peaks and two cross-peaks are still clearly visible.

The presence of off-diagonal peaks in the 2D spectrum confirms our assumption that the water O–D stretch vibration exhibits a different behavior at the surfactant interface compared to the air–water interface, where a signal was observed only along the diagonal. The presence of an off-diagonal intensity shows that the localized and delocalized modes are coupled and the excited population in one mode is rapidly transferred to the other mode. Additionally, we can see that the localized and delocalized modes do not decay to the ground state on the same time scale. The higher frequency, localized, mode takes longer to reach the ground state than the delocalized mode at low frequencies. This is most clearly seen by comparing the relative intensities of the diagonal peaks in Figure 4f,g, and is consistent with previous observations at the water–charged lipid interfaces.[33,34] Compared to the static spectrum (Figure 2b), it is interesting to note that the diagonal and cross-peaks in the 2D spectra (Figure 4) are slightly shifted from 2380 and 2510 cm^{-1} to 2300 and 2560 cm^{-1}. This is likely due to self-heterodyning effects; see the Supporting Information for more details. The lower right cross-peak, corresponding to the population moving from the localized to the delocalized O–D stretch mode, is significantly larger than the upper left cross-peak. Apparently, for the localized mode, coupling to the delocalized mode is a major relaxation pathway, while in the reverse direction it is less significant. This will be explained in detail below.

Additional insights into the dynamics can be obtained from the 2D data by looking at the bleach intensity at specific frequencies as a function of the pump–probe time delay. Figure 5a,b compares the time-dependent bleach when the two different modes are excited. In each case the graph shows the intensity of both the initially excited (diagonal) peak and the peak that was not excited, i.e., the cross-peak in the 2D spectrum. The bleach is largest close to zero pump–probe time delay, where the O–D stretching vibration of the molecules is excited by the pump pulse. At later pump–probe delays the molecules start to decay back to the ground state, via an intermediate dark state,[33] so the bleach recovers. At long pump–probe time delays the molecules have decayed back to the ground state, but the molecules are now in a warmer environment, leading to a long-time signal offset. This whole process can be described by a four-level system, if the hot ground state is considered a different level compared to the original ground state.[55] However, in this interface we have two types of water. If we consider the strongly hydrogen bonded water completely distinct from the weakly hydrogen bonded

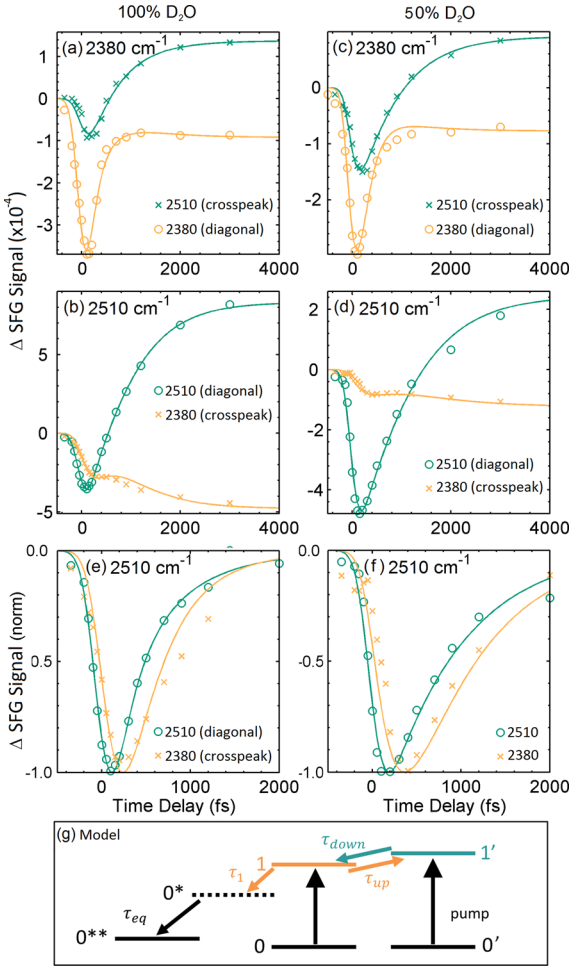

Figure 5. Time-resolved data and a cartoon of the model. (a–d) Time-resolved bleach with calculations using the model for the pure (100 % D) (a–b) and isotopically diluted (50 % D) (c–d) water. The frequency label indicates the excitation frequency. Circles indicate the excitation and detection frequencies are the same (on-diagonal), and crosses indicate the excitation and detection frequencies are different (cross-peaks). (e, f) Heat-corrected and normalized diagonal and cross-peak intensity pumped at 2510 cm^{-1} for the pure (e) and isotopically diluted (f) water with associated model calculations. (g) Model used to describe the time-resolved bleach (see also eq 2). The time-resolved data traces were taken from the time-resolved difference spectra after excitation at 2540 and 2370 cm^{-1}. These were averaged over two 60 cm^{-1} regions: centered at 2530 and 2365 cm^{-1} in the detection frequency axis. All the extracted time scales can be found in Table 1.

water, then we should have eight levels: four for each type of water. The description of the data using this model can be further simplified, as two of the states turn out to be redundant. The resulting model is summarized in Figure 5g. We excite from the ground state (0 and 0′ for the two modes) to one of the vibrationally excited states (1 and 1′). These states are coupled to each other, and energy transfer can go in both directions (as seen by the cross-peaks in the 2D spectrum). The time scales associated with this coupling are described by τ_{up} and τ_{down}. The delocalized vibrational state (1) decays to an intermediate state (0*) with lifetime τ_1. It was found from modeling the data that the inclusion of the relaxation pathway from the localized vibrational state (1′) directly to the ground state does not improve the description of the data. Apparently,

DOI: 10.1021/jacs.5b07845
J. Am. Chem. Soc. 2015, 137, 14912–14919

the probability of molecules relaxing along the 1′−0*′ pathway is rather small, implying that the time scale $\tau_{1'}$ is substantially larger than τ_{down}. By including in the model the relaxation pathway from the localized vibrational state (1′), the lifetime $\tau_{1'}$ was estimated to be at least 6 times larger than τ_{down}. This allowed us to remove the dark and hot ground states associated with the weakly hydrogen bonded water molecules from the model. From the intermediate state, the population moves back to a hot ground state (0**) with time constant τ_{eq}. Equation 2 shows the set of differential equations describing the vibrational energy transfer when the molecules are excited to the delocalized excited state (1).

$$\frac{dN_0}{dt} = -\sigma G(t)(N_0 - N_1)$$

$$\frac{dN_1}{dt} = \sigma G(t)(N_0 - N_1) + \frac{N_{1'}}{\tau_{down}} - \frac{N_1}{\tau_{up}} - \frac{N_1}{\tau_1}$$

$$\frac{dN_{1'}}{dt} = \frac{N_1}{\tau_{up}} - \frac{N_{1'}}{\tau_{down}}$$

$$\frac{dN_{0*}}{dt} = \frac{N_1}{\tau_1} - \frac{N_{0*}}{\tau_{eq}}$$

$$\frac{dN_{0**}}{dt} = \frac{N_{0*}}{\tau_{eq}} \quad (2)$$

The population in vibrational state x (x = 0, 0*, 0**, 1, 0′, 1′) is depicted by N_x. The temporal intensity profile of the excitation pulse is approximated by a Gaussian envelope ($G(t)$) with a full width at half-maximum of 300 fs. The product of the Gaussian amplitude and the cross-section (σ) was chosen such that the typical bleach signals were reproduced. Typical bleach signals, as a percentage of the total SFG signal, were obtained by dividing the pumped by the unpumped time-resolved spectra. To model the dynamics when the molecules are excited to the other state (1′), the excitation term $\sigma G(t)(N_0 - N_1)$ is simply changed to $\sigma G(t)(N_{0'} - N_{1'})$, so the population is transferred to the higher lying state (1′). The time-dependent SFG intensities recorded at the two different frequencies can be calculated from the population in the ground state and intermediate state (analogous to bulk IR pump−probe measurements[55] assumed to have the same spectral signature as the ground state), minus the stimulated emission from the excited state, according to[33]

$$\Delta\mathrm{SFG}(t) = S(((1 - r)(N_0 + N_{0*} - N_1) + r(N_{0'} - N_{1'}) + O_{hot}N_{0**})^2 - 1^2) \quad (3)$$

$$\Delta\mathrm{SFG}'(t) = S(((1 - r')(N_{0'} - N_{1'}) + r'(N_0 + N_{0*} - N_1) + O'_{hot}N_{0**})^2 - 1^2) \quad (4)$$

for the low- and high-frequency peaks, respectively. Note again that the nonresonant contribution is not included in the above equations, as it is negligible in our case. S is a scaling factor related to the total SFG signal amplitude. This factor is necessary as we are modeling the difference (pumped − unpumped) signal rather than the divided (pumped/unpumped) signal. The signal intensity ΔSFG is therefore also related to many time-independent factors, for example, the acquisition times for both the sample and the reference spectra and the oscillator strength of the transitions, which all together can be accounted for by this simple scaling factor. The factors r and r' appear in the equations to account for the spectral overlap of the two resonances: When we look at the static and 2D spectra, we see that the two peaks are broad and overlapping. The diagonals and cross-peaks are not clearly separated but overlap substantially. When we model the intensity of the diagonal peak, we may expect some intensity from the tail of the cross-peak or vice versa. To estimate this contribution, the Lorentzian fit of the static spectrum shown in Figure 3b was used. For the binning region 2335−2395 cm^{-1} used to obtain the low-frequency time-resolved traces,[1] the ratio of the area under the high-frequency Lorentzian to the area under the low-frequency Lorentzian was r = 0.10. Likewise, for the high-frequency detection region, the ratio (r') was found to be 0.11. The offset at long times due to heat is accounted for by the population of the hot ground state multiplied by the amplitude of the heat signal (O_{hot}). Since we plot the difference between the pumped and unpumped SFG signals, we subtract from the final calculated signal the signal generated with the population in the ground state, which is fully occupied, represented by the term -1^2. The calculations are shown as solid lines in Figure 5, where a global fit was performed; i.e., all kinetic parameters were the same for the description of the different experiments.

A summary of the inferred time scales can be seen in Table 1. From the calculation it was found that the energy coupling between the two states had time constants of τ_{down} = 245 fs and τ_{up} = 1 ps. Boltzmann's law would predict that $\tau_{up}/\tau_{down} = \exp(\Delta H/k_B T)$ = 1.9, where ΔH is the difference in energy (130 cm^{-1}), k_B is Boltzmann's constant, and T is the temperature (283 K). The ratio estimated from Boltzmann's law is much lower than the ratio of τ_{up}/τ_{down} = 4.1 obtained from the fitted time constants (τ_{down} = 245 fs and τ_{up} = 1 ps). A possible explanation could be that the delocalized mode has higher entropy, and this skews the coupling in favor of the delocalized mode; it is more favorable for energy to move from a localized vibration to a delocalized vibration than vice versa, leading to a larger ratio. In the case in which the vibrational quanta move from a localized mode to another localized mode, the ratio of the forward and backward transfer of the vibrational quanta is governed solely by the energy difference between the modes. On the other hand, if the vibrational quanta are converted from a localized mode to a mode that is delocalized over multiple chromophores and shows an excitonic nature, the vibrational quanta will have an entropic penalty upon moving back to a single chromophore, where localization occurs. The delocalized mode (2380 cm^{-1}) decays to the intermediate state (0*) in around τ_1 = 240 fs. The hot ground state grows in with τ_{eq} = ~700 fs, which is in good agreement with the time constant for the thermalization process.[56]

Table 1. Time Scales Extracted from a Global Optimization of Different Data Sets Using the Coupled Differential Equations Model

	τ_{down} (fs)	τ_{up} (ps)	τ_{up}/τ_{down}	τ_1 (fs)	τ_{eq} (fs)
100% D/(D + H)	245	1	4.1	240	700
50% D/(D + H)	670	2.7	4.1	270	700

We repeated these time-resolved measurements with isotopically diluted water. If τ_{down} and τ_{up} remain unchanged, this would indicate that the change in vibrational frequency is

DOI: 10.1021/jacs.5b07845
J. Am. Chem. Soc. 2015, 137, 14912−14919

governed by a change of the local environment of the excited molecule, i.e., spectral diffusion resulting from structural dynamics. Upon isotopic dilution, the hydrogen bond dynamics take place on similar time scales for the two isotopes,[57,58] so that if spectral diffusion is caused by hydrogen bond forming and breaking, the time scales should remain largely unchanged. If, however, the coupling times in isotopically diluted water are significantly longer, the coupling comes from the inter- or intramolecular energy transfer via dipole−dipole coupling,[41,59] because isotopic dilution reduces the density of O−D oscillators in the sample, and thereby increases the average distance, lowering the probability of energy transfer. In Figure 5c,d we see the time-resolved bleach of SDS dissolved in 50% isotopically diluted water. Clearly, the coupling times increase substantially: the downhill coupling time increases to τ_{down} = 670 fs, and the uphill to τ_{up} = 2.7 ps. This slowing down is already apparent from the raw data. The diagonal bleach and cross-peak bleach versus pump−probe delay time, as seen in Figure 5c,d, have been corrected for the thermal effects and normalized, and replotted in Figure 5e,f. The time delay between the (green) diagonal and the (orange) cross-peak ingrowth is clearly larger in the isotopically diluted water (f) than in the pure water (e). This shows that energy transfer is the dominant coupling mechanism, consistent with the short coupling time scale. Remarkably, the τ_1 lifetime is relatively insensitive to isotopic dilution compared to bulk water.[41] From the 2D time-resolved measurements we infer both that the delocalized and localized modes are strongly coupled and that rapid inter- or intramolecular energy transfer is the dominant coupling mechanism between these two spectral regions. This is in contrast to water at the positively charged surfactant interface,[39] where (much less prominent) cross-peaks originate from the Fermi resonance. We have shown that, for the negatively charged SDS interface, the cross-peaks do not originate from the Fermi resonance, both from the isotopically diluted static spectral peak intensities (Figure 3) and from the ultrafast energy transfer dynamics (Figure 5). This shows that the charge of the surfactant headgroup has a large effect on the interaction of that headgroup with the interfacial water molecules.

In summary, we find two coupled types of O−D stretch vibrations at the water−negatively charged surfactant−air interface: a lower frequency delocalized mode that originates primarily from the aligned water molecules below the surfactant monolayer, and a localized mode with higher frequency originating from more isolated water molecules in direct contact with the SDS molecules. Various spectroscopy[60,61] and theoretical[38,45] studies have shown that water molecules in the presence of an anion vibrate at higher frequencies. Therefore, the presence of two distinct subensembles of interfacial water may be a more general phenomenon for surfactant and lipid interfaces containing a negative charge. Following vibrational excitation, the delocalized mode can relax very rapidly back to the ground state, and both modes are coupled to each other on a subpicosecond time scale. These distinct modes cannot be distinguished at the water−air interface[7,53,62] in the absence of a surfactant, or in the presence of a positively charged surfactant;[39] therefore, the anionic SDS surfactant monolayer seems to fundamentally change the behavior of the water molecules when compared to other aqueous interfaces.

EXPERIMENTAL METHODS

Static and Time-Resolved 2D-SFG. The sum frequency signal was generated by focusing a broad-band IR beam (p-polarized, 5 μJ, 550 cm^{-1} fwhm, centered at 2300 cm^{-1}, angle 40° to normal) and a narrow-band visible beam (s-polarized 15 μJ, 15 cm^{-1} fwhm, centered at 792 nm, angle 70° to normal) on the water sample. To avoid heating of the surface by the laser beams,[63] a rotating trough is used, rotating sufficiently quickly so that every laser shot probes a new surface spot. The reflected sum frequency (s-polarized, centered at 670 nm light) was sent to the spectrometer and detected with an electron-multiplying charge-coupled device (CCD) camera. The phase-resolved (heterodyne) SFG spectra were measured on a different setup, the details of which can be found in ref 52. To record the time-resolved 2D spectrum, the water sample was excited with a narrow-band (p-polarized, ∼ 80 cm^{-1} fwhm, angle 55° to normal) IR pulse, which excited a subset of the water molecules to a higher vibrational level. Two SFG spectra were recorded—one with and one without the excitation pulse present—the difference showing how the excitation of specific molecules affects the surface response. Changing the pump−probe time delay allowed us to observe how the excited population changed in time. A 2D spectrum at each time delay was built by varying the pump frequency. Difference SFG spectra were measured at 23 different pump−probe time delays between −1 and +20 ps, and at 9 different pump frequencies (2220, 2300, 2370, 2410, 2470, 2540, 2570, 2600, and 2680 cm^{-1}). The pump intensity varied between 0.7 and 5 μJ. The trough was cooled to 283 K to reduce evaporation. Water was added from a reservoir as it evaporated to keep the height stable throughout the measurement. Details on how the difference spectra were combined to construct a 2D-SFG spectrum can be found in the Supporting Information. The experiment was conducted several times to ensure reproducibility.

SDS Solution Preparation. The SDS surfactant was purified as detailed in ref 64 to remove the dodecanol, which is known to be a degradation product of SDS[65,66] (see the Supporting Information for more details). The experiment was repeated with unpurified (as-received) SDS and with pure dodecanol to ensure the observed water dynamics were solely due to the surfactant and not due to any impurities (see the Supporting Information for the dodecanol results). The SDS was dissolved in D_2O in a 12 mM solution, with 10 mM NaCl. A concentration of 12 mM was chosen as it is above the critical micelle concentration, which reduces the surface propensity of dodecanol impurities. In addition, a new SDS solution was created every 3 days to reduce the probability of dodecanol impurities in the solution due to SDS breakdown.[65] The isotopically diluted solutions were created by first making pure solutions in D_2O and H_2O and then mixing the two solutions with the correct proportions.

ASSOCIATED CONTENT

Supporting Information

The Supporting Information is available free of charge on the ACS Publications website at DOI: 10.1021/jacs.5b07845.

Details about the 2D-SFG analysis, details about and measurements for dodecanol impurities in SDS, and a discussion on Fresnel corrections for static SFG spectra (PDF)

AUTHOR INFORMATION

Corresponding Author

*Ruth.Livingstone@mpip-mainz.mpg.de.

Notes

The authors declare no competing financial interest.

ACKNOWLEDGMENTS

We thank Z. Zhang for her assistance with the 2D-SFG technique, S. Hosseinpour and S. Schmitt for assistance with the ATR measurements, M. Knecht for purifying the SDS

DOI: 10.1021/jacs.5b07845
J. Am. Chem. Soc. 2015, 137, 14912−14919

samples, and both R. K. Campen and J. Hunger for helpful discussions. R.A.L. thanks the Humboldt Foundation for generous funding.

REFERENCES

(1) Smulders, E.; von Rybinski, W.; Sung, E.; Rähse, W.; Steber, J.; Wiebel, F.; Nordskog, A. Laundry Detergents. *Ullmann's Encyclopedia of Industrial Chemistry*; Wiley-VCH: Weinheim, Germany, 2000.
(2) Tahara, T.; Kanatani, K. *FEMS Microbiol. Lett.* **1997**, *147*, 287.
(3) Nihonyanagi, S.; Yamaguchi, S.; Tahara, T. *J. Chem. Phys.* **2009**, *130*, 204704.
(4) Mondal, J. A.; Nihonyanagi, S.; Yamaguchi, S.; Tahara, T. *J. Am. Chem. Soc.* **2010**, *132*, 10656.
(5) Mysels, K. J. *Langmuir* **1986**, *2*, 423.
(6) Shen, Y. *Nature* **1989**, *337*, 519.
(7) Zhang, Z.; Piatkowski, L.; Bakker, H. J.; Bonn, M. *Nat. Chem.* **2011**, *3*, 888.
(8) Singh, P. C.; Nihonyanagi, S.; Yamaguchi, S.; Tahara, T. *J. Chem. Phys.* **2012**, *137*, 094706.
(9) Knock, M. M.; Bell, G. R.; Hill, E. K.; Turner, H. J.; Bain, C. D. *J. Phys. Chem. B* **2003**, *107*, 10801.
(10) Ward, R. N.; Duffy, D. C.; Davies, P. B.; Bain, C. D. *J. Phys. Chem.* **1994**, *98*, 8536.
(11) Johnson, C. M.; Tyrode, E. *Phys. Chem. Chem. Phys.* **2005**, *7*, 2635.
(12) Bonn, M.; Bakker, H. J.; Tong, Y. J.; Backus, E. H. G. *Biointerphases* **2012**, *7*, 20.
(13) Mondal, J. A.; Nihonyanagi, S.; Yamaguchi, S.; Tahara, T. *J. Am. Chem. Soc.* **2012**, *134*, 7842.
(14) Gragson, D. E.; McCarty, B. M.; Richmond, G. L. *J. Am. Chem. Soc.* **1997**, *119*, 6144.
(15) Chen, X. K.; Hua, W.; Huang, Z. S.; Allen, H. C. *J. Am. Chem. Soc.* **2010**, *132*, 11336.
(16) Gragson, D. E.; McCarty, B. M.; Richmond, G. L. *J. Phys. Chem.* **1996**, *100*, 14272.
(17) Tielrooij, K. J.; Garcia-Araez, N.; Bonn, M.; Bakker, H. J. *Science* **2010**, *328*, 1006.
(18) Schweighofer, K. J.; Essmann, U.; Berkowitz, M. *J. Phys. Chem. B* **1997**, *101*, 3793.
(19) Kawai, T.; Kamio, H.; Kon-No, K. *Langmuir* **1998**, *14*, 4964.
(20) Missel, P. J.; Mazer, N.; Benedek, G.; Young, C.; Carey, M. C. *J. Phys. Chem.* **1980**, *84*, 1044.
(21) Lu, J. R.; Purcell, I. P.; Lee, E. M.; Simister, E. A.; Thomas, R. K.; Rennie, A. R.; Penfold, J. *J. Colloid Interface Sci.* **1995**, *174*, 441.
(22) Turner, S. F.; Clarke, S. M.; Rennie, A. R.; Thirtle, P. N.; Cooke, D. J.; Li, Z. X.; Thomas, R. K. *Langmuir* **1999**, *15*, 1017.
(23) Lu, J. R.; Marrocco, A.; Su, T. J.; Thomas, R. K.; Penfold, J. *J. Colloid Interface Sci.* **1993**, *158*, 303.
(24) Dutkiewicz, E.; Jakubowska, A. *Colloid Polym. Sci.* **2002**, *280*, 1009.
(25) Casson, B. D.; Bain, C. D. *J. Phys. Chem. B* **1998**, *102*, 7434.
(26) Nihonyanagi, S.; Yamaguchi, S.; Tahara, T. *J. Am. Chem. Soc.* **2010**, *132*, 6867.
(27) Hamm, P.; Zanni, M. T. *Concepts and Methods of 2D Infrared Spectroscopy*; Cambridge University Press: Cambridge, U.K., New York, 2011.
(28) Fenn, E. E.; Wong, D. B.; Fayer, M. D. *Proc. Natl. Acad. Sci. U. S. A.* **2009**, *106*, 15243.
(29) van der Loop, T. H.; Panman, M. R.; Lotze, S.; Zhang, J.; Vad, T.; Bakker, H. J.; Sager, W. F. C.; Woutersen, S. *J. Chem. Phys.* **2012**, *137*, 044503.
(30) Cringus, D.; Bakulin, A.; Lindner, J.; Vöhringer, P.; Pshenichnikov, M. S.; Wiersma, D. A. *J. Phys. Chem. B* **2007**, *111*, 14193.
(31) Levinger, N. E.; Costard, R.; Nibbering, E. T. J.; Elsaesser, T. *J. Phys. Chem. A* **2011**, *115*, 11952.
(32) Moilanen, D. E.; Fenn, E. E.; Wong, D.; Fayer, M. D. *J. Chem. Phys.* **2009**, *131*, 014704.
(33) Bonn, M.; Bakker, H. J.; Ghosh, A.; Yamamoto, S.; Sovago, M.; Campen, R. K. *J. Am. Chem. Soc.* **2010**, *132*, 14971.
(34) Ghosh, A.; Smits, M.; Bredenbeck, J.; Bonn, M. *J. Am. Chem. Soc.* **2007**, *129*, 9608.
(35) Du, Q.; Superfine, R.; Freysz, E.; Shen, Y. R. *Phys. Rev. Lett.* **1993**, *70*, 2313.
(36) Sovago, M.; Campen, R. K.; Wurpel, G. W. H.; Muller, M.; Bakker, H. J.; Bonn, M. *Phys. Rev. Lett.* **2008**, *100*, 173901.
(37) Ohe, C.; Goto, Y.; Noi, M.; Arai, M.; Kamijo, H.; Itoh, K. *J. Phys. Chem. B* **2007**, *111*, 1693.
(38) Nagata, Y.; Mukamel, S. *J. Am. Chem. Soc.* **2010**, *132*, 6434.
(39) Inoue, K.; Nihonyanagi, S.; Singh, P. C.; Yamaguchi, S.; Tahara, T. *J. Chem. Phys.* **2015**, *142*, 212431.
(40) Rey, R.; Møller, K. B.; Hynes, J. T. *J. Phys. Chem. A* **2002**, *106*, 11993.
(41) Piatkowski, L.; Eisenthal, K. B.; Bakker, H. J. *Phys. Chem. Chem. Phys.* **2009**, *11*, 9033.
(42) Kraemer, D.; Cowan, M. L.; Paarmann, A.; Huse, N.; Nibbering, E. T. J.; Elsaesser, T.; Miller, R. J. D. *Proc. Natl. Acad. Sci. U. S. A.* **2008**, *105*, 437.
(43) Heyden, M.; Sun, J.; Funkner, S.; Mathias, G.; Forbert, H.; Havenith, M.; Marx, D. *Proc. Natl. Acad. Sci. U. S. A.* **2010**, *107*, 12068.
(44) Auer, B. M.; Skinner, J. L. *J. Chem. Phys.* **2008**, *128*, 224511.
(45) Geissler, P. L. *Annu. Rev. Phys. Chem.* **2013**, *64*, 317.
(46) Tang, X.; Koenig, P. H.; Larson, R. G. *J. Phys. Chem. B* **2014**, *118*, 3864.
(47) Chun, B. J.; Choi, J. I.; Jang, S. S. *Colloids Surf., A* **2015**, *474*, 36.
(48) Nagata, Y.; Yoshimune, S.; Hsieh, C.-S.; Hunger, J.; Bonn, M. *Phys. Rev. X* **2015**, *5*, 021002.
(49) Fenn, E. E.; Wong, D. B.; Giammanco, C. H.; Fayer, M. D. *J. Phys. Chem. B* **2011**, *115*, 11658.
(50) Bredenbeck, J.; Ghosh, A.; Nienhuys, H.-K.; Bonn, M. *Acc. Chem. Res.* **2009**, *42*, 1332.
(51) Graener, H.; Seifert, G.; Laubereau, A. *Phys. Rev. Lett.* **1991**, *66*, 2092.
(52) Hsieh, C.-S.; Okuno, M.; Hunger, J.; Backus, E. H. G.; Nagata, Y.; Bonn, M. *Angew. Chem., Int. Ed.* **2014**, *53*, 8146.
(53) Singh, P. C.; Nihonyanagi, S.; Yamaguchi, S.; Tahara, T. *J. Chem. Phys.* **2013**, *139*, 161101.
(54) Nagata, Y.; Hasegawa, T.; Backus, E. H. G.; Usui, K.; Yoshimune, S.; Ohto, T.; Bonn, M. *Phys. Chem. Chem. Phys.* **2015**, *17*, 23559.
(55) Post, S. T. v. d.; Bakker, H. J. *Phys. Chem. Chem. Phys.* **2012**, *14*, 6280.
(56) Ramasesha, K.; De Marco, L.; Mandal, A.; Tokmakoff, A. *Nat. Chem.* **2013**, *5*, 935.
(57) Fecko, C. J.; Eaves, J. D.; Loparo, J. J.; Tokmakoff, A.; Geissler, P. L. *Science* **2003**, *301*, 1698.
(58) Asbury, J. B.; Steinel, T.; Kwak, K.; Corcelli, S. A.; Lawrence, C. P.; Skinner, J. L.; Fayer, M. D. *J. Chem. Phys.* **2004**, *121*, 12431.
(59) Woutersen, S.; Bakker, H. J. *Nature* **1999**, *402*, 507.
(60) Allen, H. C.; Casillas-Ituarte, N. N.; Sierra-Hernandez, M. R.; Chen, X.; Tang, C. Y. *Phys. Chem. Chem. Phys.* **2009**, *11*, 5538.
(61) Walrafen, G. E. *J. Chem. Phys.* **1962**, *36*, 1035.
(62) Hsieh, C. S.; Campen, R. K.; Vila Verde, A. C.; Bolhuis, P.; Nienhuys, H. K.; Bonn, M. *Phys. Rev. Lett.* **2011**, *107*, 116102.
(63) Backus, E. H. G.; Bonn, D.; Cantin, S.; Roke, S.; Bonn, M. *J. Phys. Chem. B* **2012**, *116*, 2703.
(64) Song, S.-H.; Koelsch, P.; Weidner, T.; Wagner, M. S.; Castner, D. G. *Langmuir* **2013**, *29*, 12710.
(65) Bain, C. D.; Davies, P. B.; Ward, R. N. *Langmuir* **1994**, *10*, 2060.
(66) Fainerman, V. B.; Lylyk, S. V.; Aksenenko, E. V.; Petkov, J. T.; Yorke, J.; Miller, R. *Colloids Surf., A* **2010**, *354*, 8.

DOI: 10.1021/jacs.5b07845
J. Am. Chem. Soc. 2015, 137, 14912−14919